Available online at www.sciencedirect.com
SCIENCE DIRECT
International Journal of Heat and Mass Transfer 49 (2006) 4161–4170
International Journal of HEAT and MASS TRANSFER
www.elsevier.com/locate/ijhmt

Experimental and analytical study of the effect of contact angle on liquid convective heat transfer in microchannels

G. Rosengarten [a,*], J. Cooper-White [b], G. Metcalfe [c]

[a] School of Mechanical and Manufacturing Engineering, University of New South Wales, Sydney 2052, Australia
[b] Division of Chemical Engineering, University of Queensland QLD, 4072, Australia
[c] CSIRO, Melbourne 3190, Australia

Received 2 November 2005; received in revised form 23 February 2006
Available online 9 June 2006

Abstract

In this paper we examine the effect of contact angle (or surface wettability) on the convective heat transfer coefficient in microchannels. Slip flow, where the fluid velocity at the wall is non-zero, is most likely to occur in microchannels due to its dependence on shear rate or wall shear stress. We show analytically that for a constant pressure drop, the presence of slip increases the Nusselt number. In a microchannel heat exchanger we modified the surface wettability from a contact angle of 20°–120° using thin film coating technology. Apparent slip flow is implied from pressure and flow rate measurements with a departure from classical laminar friction coefficients above a critical shear rate of approximately 10,000 s^{-1}. The magnitude of this departure is dependant on the contact angle with higher contact angles surfaces exhibiting larger pressure drop decreases. Similarly, the non-dimensional heat flux is found to decrease relative to laminar non-slip theory, and this decrease is also a function of the contact angle. Depending on the contact angle and the wall shear rate, variations in the heat transfer rate exceeding 10% can be expected. Thus the contact angle is an important consideration in the design of micro, and even more so, nano heat exchangers.

Keywords: Microfluidics; Slip flow; Micro heat transfer; Heat exchanger; Contact angle; Wetting

1. Introduction

Fluid flow in microchannels has received much research interest due to its seemingly endless applications [1,2]. Up to now three main application areas have driven the research: (1) two-phase flow for ink jet printing which was probably the first microfluidic application; (2) high surface area heat sinks for high-flux computer chip cooling using multiple microchannel arrays [3]; and (3) lab-on-a-chip or micro total analytical systems that increase the speed and sensitivity of chemical processes, and often involve heating and temperature control of reagents and products [4]. The second and third application areas both involve convective heat transfer from a solid to a fluid, which is a process not well understood in microfluidic channels due to the relative dominance of surface forces over body forces. This fact has driven the recent increase in interest in convective heat transfer in microchannels, where a reliable heat transfer rate prediction method is required for efficient device design.

For macro-scale heat transfer design there are numerous well-established correlations for the Nusselt number (non-dimensional heat transfer coefficient) that depend on the flow conditions. Recently however, there has been considerable debate in the literature over the applicability of these macro-scale Nusselt number correlations to microfluidic flow [5–10]. This is due, primarily, to the large variation in experimental data, which we have plotted in Fig. 1.

* Corresponding author. Tel.: +61 2 9385 4112; fax: +61 2 9663 1222.
E-mail address: g.rosengarten@unsw.edu.au (G. Rosengarten).

0017-9310/$ - see front matter © 2006 Elsevier Ltd. All rights reserved.
doi:10.1016/j.ijheatmasstransfer.2006.02.057

Nomenclature

c_p	specific heat (J/kg K)
D_h	hydraulic diameter, equals 2 W in parallel plates (m)
f	friction factor
$\bar{h}$	convective heat transfer coefficient (W/m^2 K)
H	width of channel
L	length of channel
$\dot{m}$	mass flow rate (kg/s)
Nu_{Dh}	Nusselt number based on hydraulic diameter
P	pressure (Pa)
Pe	Peclet number = $Re\,Pr$
Pr	Prandtl number = $c_p\mu/\kappa$
q''	heat flux (W/m^2)
Re_{Dh}	Reynolds number based on the hydraulic diameter
T	temperature (K)
u	velocity (m/s)
w	half the height of channel (m)
W	channel height (m)
x	coordinate in width direction (m)
y	coordinate in height direction (m)
z	coordinate in flow direction (m)

Greek symbols

κ_s, κ_f	solid and fluid thermal conductivity (W/m K)
μ	liquid viscosity (Pa s)
$\dot{\gamma}$	shear rate (s^{-1})
λ	wall conduction number (see Eq. (6))

Subscripts

m	mean value
c	centreline value
hf	uniform heat flux
s	slip
T	uniform temperature
w	wall

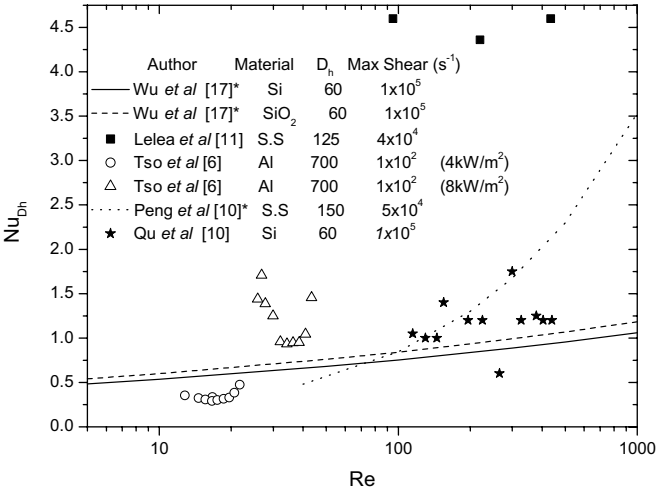

Fig. 1. Comparison of Nusselt number as a function of Reynolds number for laminar convective liquid heat transfer in microchannels. S.S = stainless steel, contact angle 75°, Al contact angle 70°, Silicon 20°–80° depending on processing steps, $SiO_2 \leqslant 20°$. The asterix alongside the reference denotes that conditions of test were not thermally fully developed.

The fully developed macro-scale laminar Nusselt number based on the hydraulic diameter, Nu_{Dh} is known to be constant, with values between approximately 3 and 8 depending on the channel cross sectional shape and the boundary condition. As Fig. 1 shows, most of the current experimental data is far from constant or even close to the expected values except for the result of Lelea et al. [11] which is for a relatively low shear rate. There are various reasons for the lack of consistency in the experimental data, but most are due to the following:

- Approximations and assumptions made (such as linear interpolation of the difference between inlet and outlet temperatures) due to the difficulty in measuring bulk fluid temperatures. It is almost impossible to place a temperature sensor in a microchannel without effecting the flow [12,13].
- Entrance effects dominating the heat transfer [14].
- Heat loss due to the increased surface area to volume ratio in microchannels relative to macro-channels [15].
- Relative dimensional tolerances in fabrication leading to higher dimensional uncertainties than those in macro-channels.
- Axial conduction, due to the thickness of the wall relative to the channel dimension, destroying assumed ideal conditions [15,16].
- Ill-defined surface variability such as roughness and hydrophobicity [17].

While most of the points mentioned above are reasonably well understood, there is little data on the effect of contact angle on the heat transfer rate, even within the work relating contact angle to slip flow (where there exists a non-zero fluid velocity at a solid wall) and the associated reduction in pressure drop (see, for example, a recent review article by Lagua et al. on slip effects in microfluidics [18]).

1.1. Slip flow

The effect of contact angle on slip flow and pressure drop has been well documented both experimentally [19–22] and by using molecular dynamics simulations [23–25]. On the other hand, there is a lack of experimental data on the effect of the contact on the heat transfer rate. Slip

flow is an important consideration because it may allow, with careful surface property selection, a significant reduction in the friction pressure drop and thus the pumping power required for micro heat-exchangers and other microfluidic devices. While the underlying physical cause of slip is not fully understood, what is clearly known is that an apparent slip occurs more readily on non-wetting surfaces (hydrophobic), on rough surfaces, and at high shear rates. Slip may therefore become important in microchannels, as surface modification can be designed and assembled into microdevices, surface roughness becomes significant relative to the channel size, and due to their small dimensions, it is possible to obtain large shear rates (Section 2).

Molecular slip, where the fluid molecules tumble along the wall much like two solid surfaces sliding over one another, occurs when the forces between the fluid and wall molecules are not strong enough to overcome the shear forces at the wall. This decoupling of the fluid from the wall equates to lower frictional pressure drops, and similarly, we propose, to higher interfacial thermal resistance (or reduced heat-transfer coefficient).

A further reason why slip may be important in convective heat transfer is that higher temperatures may induce larger slip velocities. Ruckenstein and Rejora [26] used thermodynamic relations to show how an axial temperature gradient can have a major effect on the molecular slip by changing the chemical potential gradient at the solid/fluid interface. However, their theory is problematic: it makes the unphysical assumption of a gap between the liquid and solid molecules, and it has, as yet, no direct experimental support.

1.2. Critical shear rate for slip flow

Many studies have shown either directly or indirectly that there is a critical wall shear rate for the onset of molecular slip. The first identification of this was the molecular dynamics simulation by Thomson and Troian [24]. Experimental evidence for critical shear rates and their approximate values is summarised in Table 1. The concept of a critical shear rate is consistent with slip being observed in microchannels in certain circumstances. For a given Reynolds number, the shear rate is inversely proportional to the square of the channel height (cf. Section 2). This means that shear rates in microchannels will be much higher than in macro-channels for the same Reynolds number. This also explains why slip has not been seen in macro-size channels with the exception of Watanabe et al. [27] who observed a large pressure reduction effect in approximately 10 mm diameter tubes with a rough hydrophobic surface. The effect that they observed was probably due to the surface area reduction of the wetted wall associated with trapped air in the large surface roughness (~20 μm) and not molecular slip.

Table 1
Example of some critical shear rates extracted from the literature from which either a critical shear rate was specified, or where it has been inferred from the departure of hydrophobic and hydrophilic data

Authors	Critical shear rate (s^{-1})	Comments
Wu and Cheng [17]	~50,000	Roughness ~10 nm
Zhu and Granick [20]	~10,000	Roughness ~10 nm
Choi et al. [19]	~10,000	Roughness <5 nm

1.3. Contact angle and heat transfer

Given that the contact angle of a liquid affects frictional pressure drop, it is likely that it will also affect the convective heat transfer rate. There have been investigations using molecular dynamics simulations [25,28,29] of a stagnant fluid sandwiched between two solids, that show the existence of a temperature jump between a wall and a fluid (i.e. an interface thermal resistance) that increases markedly with contact angle. The temperature jump due to slip is well established in rarefied gases, (see for e.g. [30,31]), but the effect of slip on heat transfer in liquids is different because the fluid/wall interaction is the dominant factor.

There is only one experimental study that reports the effect of contact angle on the convective heat transfer rate in microchannels [17]. That study is limited to comparing flow inside silicon and silicon dioxide microchannels, and it shows a decrease in the pressure drop and the Nusselt number for the silicon microchannels, which are more hydrophobic, of up to approximately 10% relative to the silicon dioxide channels (depending on the Reynolds number). While the authors give no associated explanation for this variation in behaviour it is probably due to slip flow.

Given that apparent slip reduces pressure drop, in this paper we investigate the effect of the contact angle on the heat transfer rate using a specially designed heat exchanger where the surface contact angle can be varied reliably. We simultaneously measure the heat transfer rate and the pressure drop to test for a relationship between the effect of contact angle on pressure drop and heat transfer rate.

2. Theory

Consider the parallel geometry in Fig. 2 that shows a schematic of the temperature and velocity profile between parallel plates that can be essentially regarded as two-dimensional. The velocity profile for flow between parallel plates with no-slip is given by [32]

$$\frac{u}{u_c} = \left(1 - \left(\frac{y}{w}\right)^2\right), \tag{1}$$

where u is the fluid velocity, u_c is the channel centreline velocity (maximum velocity), y is the vertical coordinate with its origin at the centre of the channel, and w is half the channel height. The maximum shear rate occurs at the wall and can be written as

$$\left.\frac{du}{dy}\right|_{y=w} = \dot{\gamma}_{max} = \frac{3u_m}{w} = \frac{3Re_{Dh}v}{2w^2}, \tag{2}$$

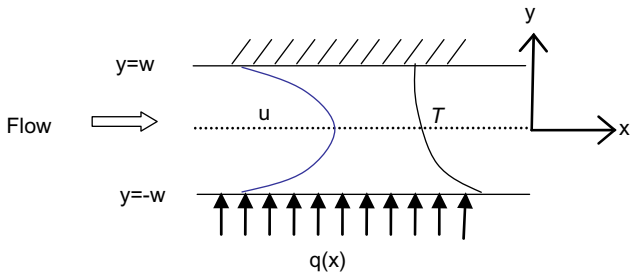

Fig. 2. Schematic of ideal 2D flow and heat transfer (q) between parallel plates showing velocity (u) and temperature (T) profiles.

where Re_{Dh} is the Reynolds number based on the hydraulic diameter, $D_h = 2w$, and v is the kinematic viscosity. Eq. (2) illustrates the fact that for a fixed Reynolds number the maximum shear rate scales as the reciprocal of the channel height squared.

The incorporation of a slip velocity as a boundary condition to solve the Navier–Stokes equations is often used (e.g. [19]). To examine how a slip velocity would affect the fully developed Nusselt number we can rewrite Eq. (1) to include a slip velocity, u_s

$$u = u_c\left(1 - \left(\frac{y}{w}\right)^2\right) + u_s. \tag{3}$$

Using Eq. (3) in the energy equation one obtains a non-dimensional temperature profile (for a derivation see Appendix A) given by

$$\frac{T_{fw} - T}{T_{fw} - T_{w2}} = \frac{1}{\left(\frac{4}{3} + 2\frac{u_s}{u_c}\right)}\left[\frac{13}{12} - \frac{1}{2}\left(\frac{y}{w}\right)^2 + \frac{1}{12}\left(\frac{y}{w}\right)^4 + \frac{2}{3}\left(\frac{y}{w}\right) + \frac{u_s}{u_c}\left(\frac{3}{2} - \frac{1}{2}\left(\frac{y}{w}\right)^2 + \left(\frac{y}{w}\right)\right)\right]. \tag{4}$$

Eq. (4) shows that for constant heat flux and driving pressure the effect of slip is to decrease the temperature of the fluid, with the maximum decrease being near the centre (about 1% for a relative slip velocity of 10%). This effect is shown in Fig. 3.

The fully developed Nusselt number for slip flow is given by (see Appendix A)

$$Nu_{Dh} = \frac{4\left(\frac{4}{3} + \frac{2u_s}{u_c}\right)^2}{\left[1.32 - \frac{u_s}{u_c}\left(3.7 + \frac{8}{3}\frac{u_s}{u_c}\right)\right]}. \tag{5}$$

Eq. (5) shows that when the slip velocity is zero, the Nusselt number is equal to the standard no-slip value of 5.35 for flow between parallel plates [32]. Given that in the derivation of Eq. (5) we have fixed the heat flux at the wall and the wall temperature as boundary conditions, the net temperature change of the fluid decreases due to the increased net flow rate for the same pressure drop. In reality the wall temperature would not be fixed, and it would be expected to increase due to the increased thermal resistance between the wall and the fluid. Fig. 4 shows the relative change in the fully developed Nusselt number (Eq. (5)), for different values of the slip velocity, induced by the increased flow rate. For example the Nusselt number increases by approximately 2% for a 10% ratio of slip velocity to centre line velocity.

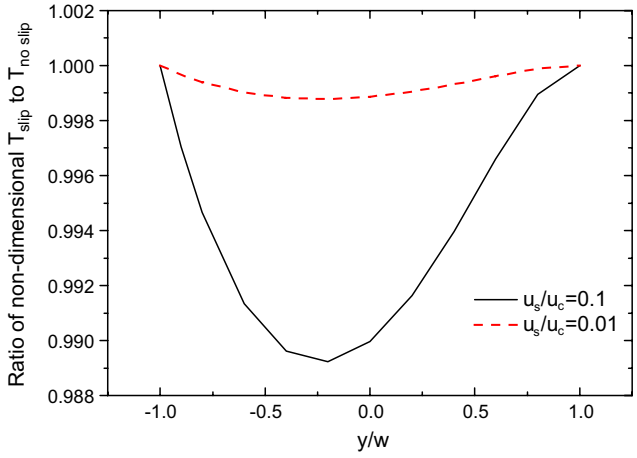

Fig. 3. Effect of slip on the non-dimensional temperature profile for two different slip velocities.

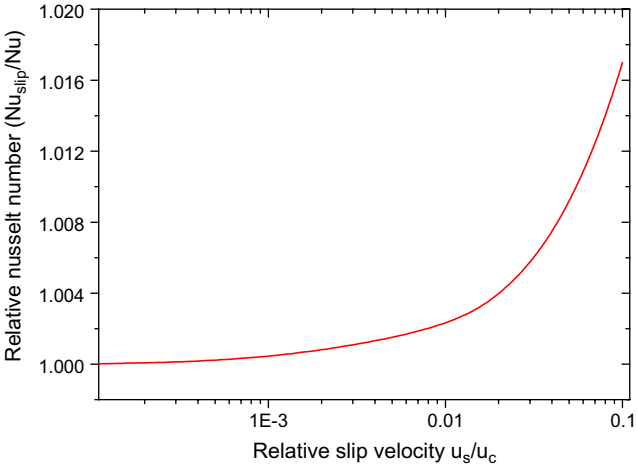

Fig. 4. Relative change in the Nusselt number due to slip-induced flow-rate variations only (from Eq. (5)).

3. Experiments

In the experiments we want to produce the conditions most conducive to slip, which are high shear rates and high contact angle (hydrophobic) surfaces. Fig. 5 shows the schematic designs of the heat exchanger and the measurement system. The heat exchanger channel width is much greater than its depth (aspect ratio 10^2), in order to reduce the effects of sidewalls and has one wall at a constant heat flux (or temperature depending on the flow rate) while the other wall is adiabatic. This is a well-studied geometry (parallel plates) for which the Nusselt number is a constant 5.35 for constant heat flux or 4.86 for constant temperature boundary conditions.

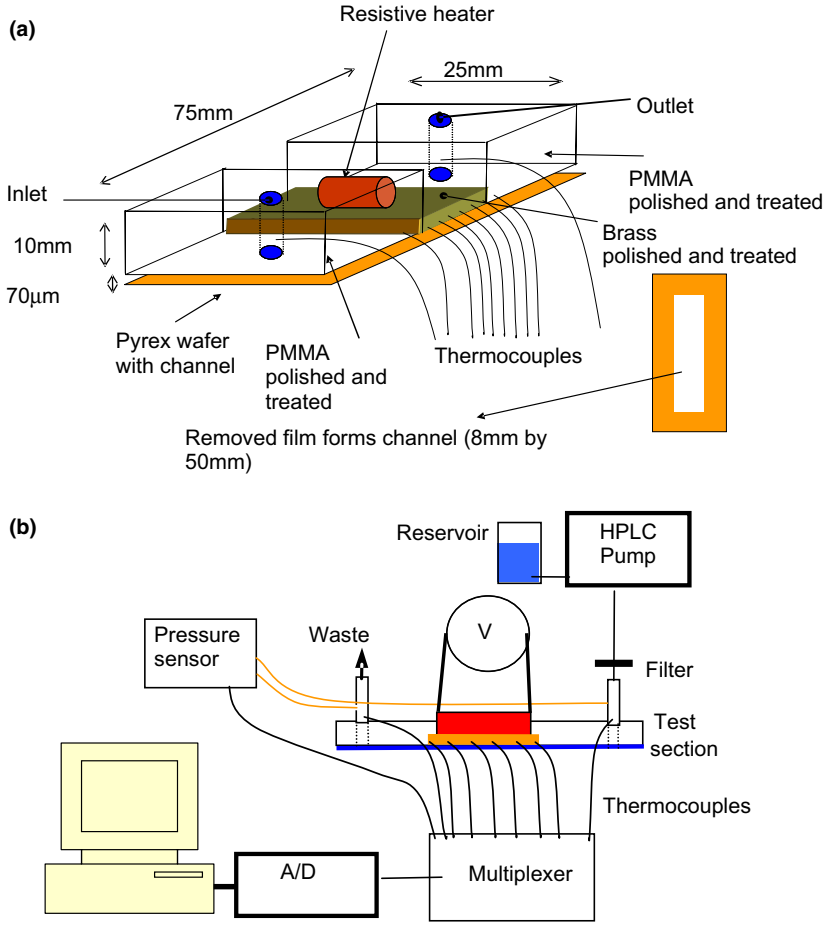

Fig. 5. (a) Schematic diagram of heat exchanger and (b) schematic of experimental setup.

The heat transfer surface consists of 2 mm thick brass imbedded into a Poly(methyl methacrylate)—PMMA or its trade name Perspex—base and polished flat using a Logitech PM5 precision lapping and polishing machine. The RMS roughness of the brass, measured by an atomic force microscope, was found to be approximately 50 nm (Fig. 6) and less than half of this for the PMMA. The channels were made by attaching an adhesive film onto a microscope slide and cutting the channel out using a template. The glass slide with channel was clamped to the heat exchanger to seal. The channel depth was measured with a microscope after sealing. Heating was provided by a 10 W 47 Ω. resistor bonded to the back of the brass using high thermal conductivity epoxy (Tra-Con 2902) and heated with a calibrated HP power supply. Six 70 μm diameter type T thermocouples were imbedded in the brass, and one thermocouple was imbedded on each side of the brass in the PMMA, with their tips at the centre of the channel. Small diameter wires were used to minimise conduction losses. A thermocouple was also placed at the centre of the inlet and outlet channels.

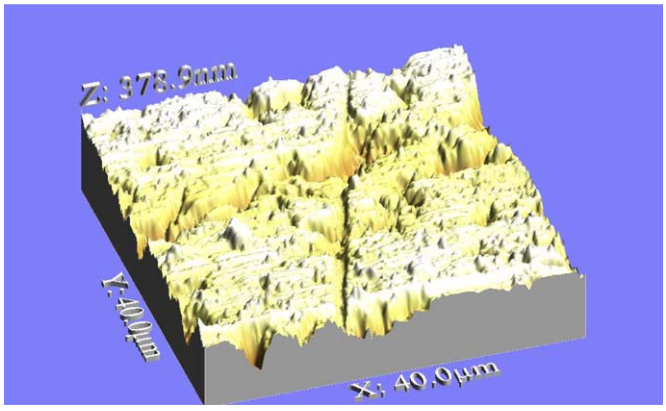

Fig. 6. Atomic force microscope image of a section of polished brass (RMS roughness approximately 50 nm).

The temperature measurement system was calibrated against a traceable platinum resistance thermometer in a uniform temperature water bath. Pressure measurements were made with a calibrated Honeywell 26PC01KOxxa pressure sensor. Data was captured to computer via a high precision National Instruments 4350 16 bit data logger via constant temperature terminal block. An Alltech 626 HPLC pump with a flow rate range of 0.001 to 12 ml/min was used for continuous pumping. Estimated uncertainties in the measurements are given in Table 2.

Table 2
Uncertainties in measured quantities

Value	Uncertainty
Pressure (Pa)	150 + 2%
Temperature (K)	0.15
Flow rate (ml/min)	2%
Channel height (μm)	3

The heat exchanger surface contact angle was varied by depositing thin layers of various materials on both the top of bottom channel surfaces using either plasma polymer deposition [33] or electron beam evaporation. The hydrophobic polymer was perfluorocyclohexane with a contact angle of 120° measured with OCA surface tensiometer. The polymer thicknesses were measured to be approximately 10–20 nm which, with the heat fluxes used, gave a negligible temperature drop. The hydrophilic layer was 50 nm SiO_2 with a contact angle of less than 20°. The working fluid was triply distilled water that was degassed prior to use, and the complete heat exchanger was insulated with 2 cm thick polystyrene. The heat input ranged from approximately 0.2 W to 5 W depending on the flow rate in order to keep a temperature difference between 7 and 25 °C and minimise differential thermal expansion.

3.1. Axial conduction

Axial conduction, which is the heat that is conducted axially along a channel wall instead of into the fluid, can be significant in microfluidics because the channel walls often have a considerably larger cross sectional area than the fluid channels. Numerical simulations of our system using CFD-ACE[1] showed that, even for the largest experimental flow rates, the wall boundary condition never reaches uniform heat flux conditions [34]. Subsequent experiments and numerical simulations found that significant heat was being transferred axially along the wall.

The ratio of conduction heat transfer through a channel wall, to the convective heat transfer to the fluid from the wall, assuming the same temperature difference for the two processes, has been presented previously as a non-dimensional number to define compact heat exchanger efficiency [35] (see Eq. (3)). This number, re-arranged, has been recently applied to microfluidics and is given by [35]:

$$\lambda = \frac{A_s D_h \kappa_s}{A_f L \kappa_f} \frac{1}{Pe}, \tag{6}$$

where A_s and A_f are the cross sectional areas of the solid wall and fluid respectively, L is the channel length, κ is the thermal conductivity, and Pe is the Peclet number given by $Re_{Dh}Pr$.

Given a uniform heat flux on a channel outer wall, for low values of λ (<0.01) axial conduction can be considered negligible, and the fluid/solid surface boundary condition will be close to being uniform heat flux. Conversely, for higher values of λ axial conduction becomes more important, and the boundary conditions approach uniform temperature for infinite λ. Microfluidic channels are generally characterised by large A_s/A_f and low Pe, hence the tendency for axial conduction to become significant.

An example of the heated brass-wall temperature for a low and high Pe (high and low λ) number case is shown in Fig. 7a, which contains experimental and numerical data in good agreement. For uniform wall temperature the plot would be flat, while for uniform heat flux the graph would have a linear dependence on distance. It is clear that for the higher λ case with the lower flow rate, the conditions are more like a uniform wall temperature, while for the lower λ case the conditions are neither uniform temperature nor heat flux. In either case a linear interpolation of the wall or the fluid temperature would be erroneous, and this may be why papers that have assumed this have non-standard Nusselt numbers that vary with Reynolds number. The simulated distributions of heat flux and Nusselt number for the two flow rates are shown in Figs. 7b and c. For the lower flow rate, all the heat is essentially transferred in the first 10% of the heat exchanger. After that the Nusselt number approaches the fully developed laminar value of 4.86. The higher flow rate case evolves from an almost uniform heat flux Nusselt number of approximately 5.35, to the value for uniform temperature of 4.86 when there is considerably less heat being transferred. Thus for the range of conditions to be tested, even though the external boundary condition consists of uniform heat flux, the fluid does not experience a uniform boundary condition due to varying effects of wall conduction. This common problem in microfluidics can, in the most part, be overcome by using thin film heaters and thin insulating substrates [36].

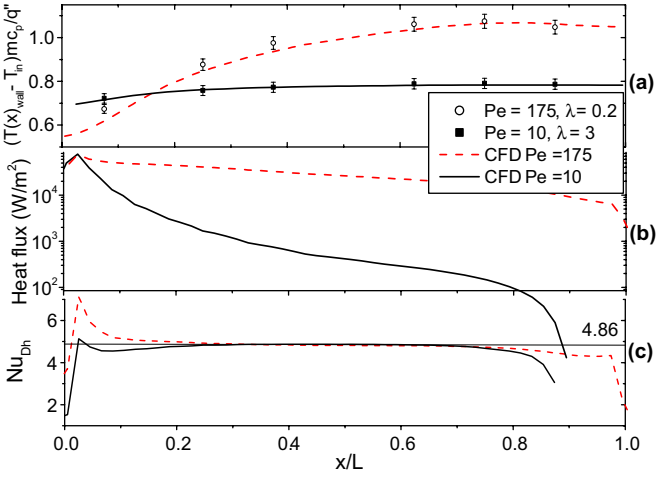

Fig. 7. (a) Non-dimensional wall surface temperature profile vs non-dimensional distance along heater, for both experiments (70° contact angle) and using CFD assuming no-slip. (b) Heat flux distribution and (c) Nusselt number distribution that has the value for constant temperature boundary conditions indicated.

[1] www.cfdrc.com

4. Results

We report measurements of the pressure drop and heat transfer rate in the micro heat exchanger for three different contact angles, in order to determine the effect contact angle has on slip and to see if this affects the heat transfer rate.

4.1. Pressure drop

Fig. 8 shows the pressure drop as a function of maximum shear rate for surfaces with contact angles of 20°, 70°, and 120° both unheated and with heating. The channel spacings for the three contact angle cases were 71 μm, 75 μm, and 72 μm, respectively. The pressure drops for the heated cases have been corrected for temperature-induced viscosity variations so that they are equivalent to the fluid being at 21 °C. The straight line in Fig. 8 represents a best fit to the data below a shear rate of 5000 s^{-1}. For pure no-slip laminar conditions the data should follow the straight line for all shear rates. The data departs from the no-slip line above a shear rate of approximately 10,000 s^{-1}, which is consistent with the critical shear rate for slip in previous studies (see Table 1). As we do not measure the velocity profile directly we can only infer apparent slip from departure of the pressure data from no-slip expectations.

Not apparent in the data of Fig. 8 above a shear rate of 10,000 s^{-1}, is the dependency of the departure from no-slip conditions on contact angle and heating. Departures from no-slip predictions increase with both contact angle and heating. Different ways to plot the data in Figs. 9 and 10 bring out this aspect of the data.

A more general way of comparing the data (with different channel dimensions) is to use the non-dimensional friction factor given by $f = \frac{\Delta P}{L} D_h / 0.5 \rho u_m^2$. Fig. 9 shows the friction factor multiplied by the Reynolds number, as a function of the Reynolds number. For no-slip, laminar flow between parallel plates, *fRe* is a constant 24. For the lower values of Reynolds number, *fRe* tends to be slightly higher than the laminar no-slip value of 24. This is most probably due to the uncertainty in the channel spacing. What is clear, however, is that for Reynolds numbers greater than approximately 20 there is a definite decrease in the data. From Fig. 9 it may be difficult to discern the effect of contact angle. To help filter out the noise in the data we have plotted the gradient of the data as the insert of Fig. 9 for Reynolds numbers greater than 20 (when the shear rate is high enough for the data to diverge from no-slip conditions). The insert plot indicates a clear dependence of the rate of friction factor decrease on the contact angle. The lower the contact angle the lower the gradient or the lower the rate of divergence from no slip conditions. For fully wetting surfaces (a contact angle of zero) we would not expect slip and thus the gradient should be zero. Interestingly there is a small difference between the heated and unheated cases which, while not being the same magnitude, is quantitatively the same predicted by the theory of Ruckenstein and Rajora [26] who quote that a temperature gradient of 4.45°/cm can produce slip magnitudes with equivalent pressure drop reductions of 1 atm/cm.

4.2. Heat Transfer

The data in Figs. 8, 9 show that the frictional pressure drop decreases due to slip above a critical shear rate, with the magnitude of the decrease depending on the contact angle. We now report on how slip affects the heat transfer rate. Fig. 10 shows the ratio of heat transferred to the fluid

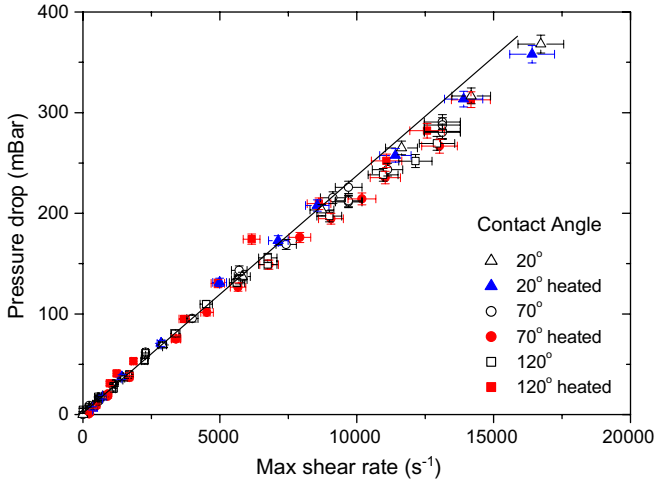

Fig. 8. Pressure drop as a function of shear rate at the wall for different contact angle cases. The straight line is a linear line of best fit for the data at shear rates less than 5000 s^{-1}.

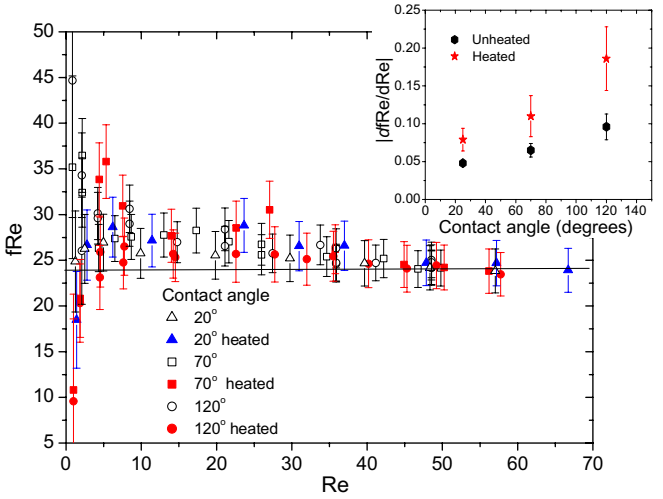

Fig. 9. Friction factor multiplied by *Re* vs *Re* for different contact angle cases. The straight line indicates the standard laminar no-slip value of 24. The insert shows magnitude of the gradient of *fRe* vs *Re* graph for values *Re* greater than 10, as a function of contact angle, for heated and unheated cases. A clear dependence of the gradient of the decrease with contact angle is shown.

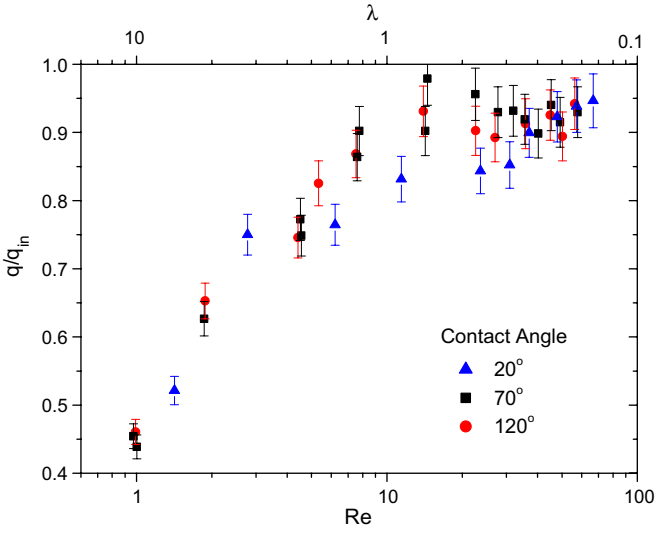

Fig. 10. Ratio of heat transfer rate to the fluid, to the heater input power as a function of wall conduction parameter, and of Reynolds number for different contact angles.

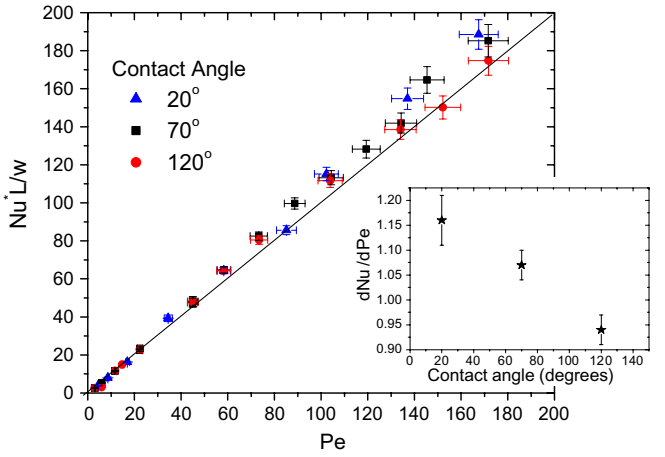

Fig. 11. Ratio of non-dimensional heat flux as a function of Pe for different contact angles. Also drawn is the theoretical line assuming uniform temperature boundary conditions with laminar no-slip flow. The insert shows the gradient of $Nu*$ vs Pe graph as a function of contact angle for $Pe > 100$. For no-slip conditions with a uniform heat flux boundary condition the gradient should be approximately 1.3.

to the electrical heat input as a function of Reynolds number or wall conduction parameter λ. The measured heat transfer rate, q, was calculated using $q = \dot{m}c_p(T_{\text{out}} - T_{\text{in}})$. As the Reynolds number increases (everything else kept constant), a larger proportion of heat is transferred to the fluid. At lower Reynolds numbers there is more chance for heat loss and a larger proportion of the heat is conducted through the solid and away from the fluid. There is little difference in the data for different contact angles apart from the 20° case ratio increasing rapidly after a Reynolds number of approximately 20 while the other two cases stabilize.

In order to compare results with slightly different conditions and geometry we will use the non-dimensional Nusselt number. As mentioned previously it is almost impossible to measure the true Nusselt number, defined in Eq. (A.9) because of the difficulty of measuring the bulk fluid temperate in microchannels. Instead we follow [37] and define a non-dimensional heat flux for no-slip conditions as

$$Nu^*_{\text{w}} = \frac{q''_{\text{mean}} W}{\kappa(T_{\text{w}} - T_{\text{in}})}, \tag{7}$$

and by assuming a uniform wall temperature,

$$Nu^*_{\text{w},T} = \frac{w\dot{m}c_p}{\kappa HL}\left(1 - \exp\left(-\frac{HL\bar{h}}{\dot{m}c_p}\right)\right) = Pe\frac{w}{L}\left(1 - \exp\left(\frac{-1}{Pe}\frac{L\bar{h}}{\kappa}\right)\right). \tag{8}$$

Given that $\bar{h}$ is very high due to the small dimensions

$$Nu^*_{\text{w},T} \approx Pe\frac{W}{L}. \tag{9}$$

Similarly we can calculate $Nu^*_{\text{w,hf}}$ assuming uniform heat flux with linear fluid and wall temperature distributions as

$$Nu^*_{\text{w,hf}} \approx Pe\frac{W}{L}\left(\frac{1}{Pe\frac{\kappa}{Lh} + 0.5}\right). \tag{10}$$

Fig. 11 shows data for $Nu^*_{\text{w}}\frac{L}{W}$ vs Pe, which, for laminar flow, with uniform temperature heat-transfer wall conditions should lie on the straight line indicated. For no-slip conditions the data will deviate from the straight line as the Peclet number increases due to the wall boundary conditions changing from uniform temperature to uniform heat flux, as seen in Fig. 7. This will increase the Nusselt number by a factor equal to the ration of Eqs. (9) and (10). At the same time slip flow will decrease the Nusselt number by lowering the heat transfer coefficient. Fig. 11 shows clearly that the departure from the uniform temperature boundary condition line for the higher contact angle case is smaller than that for the other two cases with less slip.

Similar to the pressure drop data, the effect of contact angle on the results is highlighted in the inset graph of Fig. 11 by plotting the gradient of the data for values of Peclet number greater than 100 (where slip may start to occur). This figure clearly shows the dependence on the deviation from uniform temperature boundary conditions as a function of contact angle, with the lower contact angle (hydrophilic) case having highest deviation. The gradient calculated using Eq. (10) (uniform heat flux conditions) for a Peclet number of 160 is approximately 1.3 which is very close (especially considering that we do not have uniform heat flux conditions) to the extrapolated value of zero contact angle from Fig. 11 inset. These results clearly show that the higher contact angle surfaces (hydrophobic) tend to decrease the heat transfer coefficient relative to wetting surfaces, most probably due to slip flow. The magnitude of the effect of slip is larger than predicted by Eq. (5) most probably due to an associated temperature jump with slip flow that has not been taken into account in the equation.

Given that the heat transfer coefficient decreases with slip, one would expect an associated increase in the wall temperature relative to a no-slip case due to the higher resistance to heat transfer. This is evident in Fig. 7 where the no-slip CFD results are in good agreement with the experimental results in the no-slip, low Peclet number region but are lower than experimental results for the higher Peclet number case where slip is occurring.

5. Conclusions

We have investigated the effect that liquid/surface contact angle has on the pressure drop and heat transfer rate in microfluidic channels. We have, for the first time, derived a fully developed laminar Nusselt number that takes into account the effect of having a slip velocity boundary condition. We have shown experimentally that the pressure drop decreases relative to that expected with non-slip theory above a critical shear rate and that this decrease is dependent on the contact angle. We have attributed this to slip flow that is known to occur more readily on hydrophobic surfaces and above a critical shear rate. Associated with the decrease in pressure drop is a concurrent decrease in the convective heat transfer coefficient which again is more pronounced for hydrophobic surfaces. This effect could have been overlooked previously due to the large axial conduction effect in microfluidic channels that tend to wash out more subtle effects, or due to the onset of turbulence in the larger channels at the higher shear rates. Slip flow is thus an extremely important for micro and in particular nano heat exchanger designs as heat transfer rates may decrease more than 10% at high shear rates. Surface roughness was kept at a constant 50 nm RMS so we cannot say how surface roughness interplays with these results. Further experiments are underway to reduce the uncertainties in measurement to further highlight slip effects and to include the effect of surface roughness. Future Nusselt number correlations for fully developed laminar flow in microchannels will include contact angle and shear rate.

Acknowledgements

We thank David Steele, Kevin Smeaton, Yuxun Cao for assistance, and the University of Melbourne's CSIRO collaborative grant scheme, Early Career Researcher grant scheme and RMIT VRI grant for funding.

Appendix A

Referring to Fig. 2, with fully developed flow, assuming no axial conduction, $\frac{dT}{dz} = \frac{dT_{w1}}{dz} = \frac{dT_{w2}}{dz}$ where T is the fluid velocity and the subscripts w1 and w2 refer to the two walls, and z is the axial coordinate. The governing equation for the energy balance in two dimensions becomes, with Pr the Prandlt number,

$$u\frac{dT}{dz} = \frac{v}{Pr}\frac{\partial^2 T}{\partial y^2} = u\frac{dT_{w1}}{dz}. \tag{A.1}$$

Substituting Eq. (3) into Eq. (A.1) gives

$$\frac{\partial^2 T}{\partial y^2} = \frac{Pr}{v}u_c\frac{dT_{w1}}{dz}\left[1-\left(\frac{y}{w}\right)^2+\frac{u_s}{u_c}\right]. \tag{A.2}$$

Integrating Eq. (A.2) with respect to y/w, and using the boundary condition that $\frac{\partial T}{\partial y} = 0$ at $y = w$ gives

$$\frac{\partial T}{\partial y} = \frac{Pr}{v}u_c\frac{dT_{w1}}{dz}\left[\frac{y}{w}\left(1+\frac{u_s}{u_c}\right)-\frac{1}{3}\left(\frac{y}{w}\right)^3-\left(\frac{2}{3}+\frac{u_s}{u_c}\right)\right]. \tag{A.3}$$

As we are only looking at the effect of fluid slip on the heat transfer rate, we make the assumption that even though there is velocity slip there is no temperature discontinuity at the heat flux wall. In reality we expect there to be a temperature jump at the interface of the heat transfer wall and the fluid [25,28]. Integrating again with the boundary condition at $y = -w$, $T = T_{fw}$, the fluid temperature profile is then given by

$$T_{fw}-T = \frac{Prw}{v}u_c\frac{dT_{w1}}{dz}\left[\frac{13}{12}-\frac{1}{2}\left(\frac{y}{w}\right)^2+\frac{1}{12}\left(\frac{y}{w}\right)^4+\frac{2}{3}\left(\frac{y}{w}\right)+\frac{u_s}{u_c}\left(\frac{3}{2}-\frac{1}{2}\left(\frac{y}{w}\right)^2+\left(\frac{y}{w}\right)\right)\right]. \tag{A.4}$$

Assuming that the conductivity of the fluid at the surface is equal to the bulk thermal conductivity of the fluid, k, (again, with molecular slip, this may not be the case) then with $q''_w = -k\frac{\partial T}{\partial y}\Big|_{y=-w}$ substituted into Eq. (A.3) gives $\frac{q''_w w}{k} = -\frac{Prw}{v}u_c\frac{dT_{w1}}{dz}\left(\frac{4}{3}+2\frac{u_s}{u_c}\right)$. This can be substituted into Eq. (A.4) in order to give the temperature distribution in terms of the applied heat flux, the fluid thermal conductivity and the channel dimension.

$$T_{fw}-T = \frac{\frac{q''_w w}{k}}{\left(\frac{4}{3}+2\frac{u_s}{u_c}\right)}\left[\frac{13}{12}-\frac{1}{2}\left(\frac{y}{w}\right)^2+\frac{1}{12}\left(\frac{y}{w}\right)^4+\frac{2}{3}\left(\frac{y}{w}\right)+\frac{u_s}{u_c}\left(\frac{3}{2}-\frac{1}{2}\left(\frac{y}{w}\right)^2+\left(\frac{y}{w}\right)\right)\right]. \tag{A.5}$$

If we assume that the top wall is adiabatic then at $y = w$, $T = T_{w2}$. Therefore, $T_{fw}-T_{w2} = \frac{\frac{q''_w w}{k}}{\left(\frac{4}{3}+2\frac{u_s}{u_c}\right)}\left(\frac{4}{3}+\frac{2u_s}{u_c}\right) = \frac{q'_w w}{k}$, which, when combined with (A.5) gives the non-dimensional temperature profile as a function of relative slip velocity as

$$\frac{T_{fw}-T}{T_{fw}-T_{w2}} = \frac{1}{\left(\frac{4}{3}+2\frac{u_s}{u_c}\right)}\left[\frac{13}{12}-\frac{1}{2}\left(\frac{y}{w}\right)^2+\frac{1}{12}\left(\frac{y}{w}\right)^4+\frac{2}{3}\left(\frac{y}{w}\right)+\frac{u_s}{u_c}\left(\frac{3}{2}-\frac{1}{2}\left(\frac{y}{w}\right)^2+\left(\frac{y}{w}\right)\right)\right]. \tag{A.6}$$

The mean bulk fluid temperature is given by $T_m = \frac{1}{\dot{m}}\int_A \rho u T\,dA$ where the mass flow rate is $\dot{m} =$

$\int_A \rho u \, dA = w\rho u_c\left(\frac{4}{3}+\frac{2u_s}{u_c}\right)$. As $\int_A \rho u T \, dA = \rho u_c w \int_{-1}^{1} \frac{u}{u_c}[T_{fw} - (T_{fw}-T)]\,d(\frac{y}{w})$. As we get

$$T_m = \frac{w\rho u_c}{w\rho u_c\left(\frac{4}{3}+\frac{2u_s}{u_c}\right)}\left[\left(\frac{4}{3}+\frac{2u_s}{u_c}\right)T_{fw} - 1.32\frac{\frac{q''_w w}{k}}{\left(\frac{4}{3}+2\frac{u_s}{u_c}\right)} - \frac{u_s}{u_c}\frac{\frac{q''_w w}{k}}{\left(\frac{4}{3}+2\frac{u_s}{u_c}\right)}\left(3.7+\frac{8}{3}\frac{u_s}{u_c}\right)\right]. \quad (A.7)$$

Therefore

$$T_m - T_{fw} = \frac{q''_w w}{k}\frac{1}{\left(\frac{4}{3}+\frac{2u_s}{u_c}\right)^2}\left[1.32 - \frac{u_s}{u_c}\left(3.7+\frac{8}{3}\frac{u_s}{u_c}\right)\right]. \quad (A.8)$$

Now

$$Nu_{Dh} = \frac{q'' D_h}{(T_m - T_{fw})k}, \quad (A.9)$$

where the hydraulic diameter for parallel plates is $4w$.

Substituting Eq. (A.8) into Eq. (A.9) gives the Nusselt number for uniform heat flux and pressure drop including a slip velocity, as shown in Eq. (5).

References

[1] N. Nguyen, S. Wereley, Fundamentals and Applications of Microfluidics, Artech House (2002).

[2] O. Geschke, H. Klank, P. Tellemann, Microsystem Engineering of Lab-on-a-Chip Devices, Wiley (2004).

[3] I. Madawar, Assessment of high-heat-flux thermal management schemes, IEEE Trans. Comp. Pack. Technol. 24 (2) (2001) 122–141.

[4] A. Northrup, M. Ching, R. White, R. Watson, DNA Amplification with a Microfabricated Reaction Chamber, in: 7th International Conference on Solid-State Sensors and Actuators, Yokohama, Japan, 1993, pp. 924–926.

[5] B.X. Wang, X.F. Peng, Experimental investigation on liquid forced-convection heat transfer through microchannels, Int. J. Heat Mass Transfer 37 (Special Issue) (1994) 73–82.

[6] C.P. Tso, S.P. Mahulikar, Experimental verification of the role of Brinkman number in microchannels using local parameters, Int. J. Heat Mass Transfer 43 (2000) 1837–1849.

[7] C. Sobhan, S. Garimella, A comparative analysis of studies on heat transfer and fluid flow in microchannels, Microscale Thermophys. Eng. 5 (2001) 293–311.

[8] H. Herwig, O. Hausner, Critical view on "new results in micro-fluid mechanics": an example, Int. J. Heat Mass Transfer 46 (2003) 935–937.

[9] Z.Y. Guo, Z.-X. Li, Size effect on microscale single-phase flow and heat transfer, Int. J. Heat Mass Transfer 43 (2003) 149–159.

[10] X.F. Peng, G.P. Peterson, B.X. Wang, Heat transfer characteristics of water flowing through microchannels, Exp. Heat Transfer 7 (1994) 265–283.

[11] D. Lelea, S. Nishio, K. Takano, The experimental research on microtube heat transfer and fluid flow of distilled water, Int. J. Heat Mass Transfer 47 (2004) 2817–2830.

[12] W. Qu, G. Mala, D. Li, Heat transfer for water flow in trapezoidal silicon microchannels, Int. J. Heat Mass Transfer 43 (2000) 3925–3936.

[13] W. Owhaib, B. Palm, Experimental investigation of single-phase convective heat transfer in circular microchannels, Exp. Thermal Fluid Sci. 28 (2004) 105–110.

[14] P. Lee, S. Garimella, D. Liu, Investigation of heat transfer in rectangular microchannels, Int. J. Heat Mass Transfer 48 (2005) 1688–1704.

[15] I. Tiselj, G. Hetsroni, B. Mavko, A. Mosyak, E. Pogrebnyek, Z. Segal, Effect of axial conduction on the heat transfer in microchannels, Int. J. Heat Mass Transfer 47 (2004) 2551–2561.

[16] G. Maranzana, I. Perry, D. Maillet, Mini- and micro-channels: influence of axial conduction in the walls, Int. J. Heat Mass Transfer 47 (2004) 3993–4004.

[17] H.Y. Wu, P. Cheng, An experimental study of convective heat transfer in silicon microchannels with different surface conditions, Int. J. Heat Mass Transfer 43 (2003) 2547–2556.

[18] E. Lauga, M. Brenner, H. Stone, Microfluidics: The no-sip boundary condition, in: J. Foss, C. Tropea, A. Yarin (Eds.), Handbook of Experimental Fluid Dynamics, Springer, New York, 2005.

[19] C. Choi, K. Westin, K. Breuer, To slip or not to slip-water flow in hydrophilic and hydrophobic microchannels, in: International Mechanical Engineering Conference and Exposition, New Orleans, 2002.

[20] Y. Zhu, S. Granick, Limits of hydrodynamic no-slip boundary condition, Phys. Rev. Lett. 88 (10) (2002) 106102-1–106102-4.

[21] J. Barrat, L. Bocquet, Large slip effect at a nonwetting fluid–solid interface, Phys. Rev. Lett. 82 (3) (1999) 4671–4674.

[22] D. Tretheway, C. Meinhart, Apparent fluid slip at hydrophobic microchannel walls, Phys. Fluids 14 (13) (2002) 9–12.

[23] G. Nagayama, P. Cheng, Effects of interface wettability on microscale flow by molecular dynamics simulation, Int. J. Heat Mass Transfer 47 (2004) 501–513.

[24] P. Thomson, S. Troian, A general boundary condition for liquid flow at solid surfaces, Nature 389 (1997) 360–362.

[25] L. Xue, P. Keblinski, S.R. Philpot, S.S. Choi, J. Eastman, Effect of liquid layering at the liquid–solid interface on thermal transport, Int. J. Heat Mass Transfer 47 (2004) 2004.

[26] E. Ruckenstein, P. Rajora, On the no-slip boundary condition of hydrodynamics, J. Colloid Interface Sci. 96 (2) (1983) 488–491.

[27] K. Watanabe, Yanuar, H. Udagawa, Drag reduction of Newtonian fluid in a circular pipe with a highly water-repellent wall, J. Fluid Mech. 381 (1999) 225–238.

[28] S. Maruyama, T. Kimura, A study on thermal resistance over a solid–liquid interface by the molecular dynamics method, Thermal Sci. Eng. 7 (1) (1999) 63–68.

[29] T. Ohara, D. Suzuki, Intermolecular energy transfer at a solid–liquid interface, Microscale Thermophys. Eng. 4 (2000) 189–196.

[30] S. Colin, P. Lalonde, R. Caen, Validation of a second-order slip flow model in rectangular microchannels, Heat Transfer Eng. 25 (3) (2004) 23–30.

[31] S. Yu, T. Ameel, Slip flow convection in isoflux rectangular microchannels, J. Heat Transfer, Trans ASME 124 (2002) 346–355.

[32] R.K. Shah, A.L. London, Laminar flow forced convection in ducts Adv. Heat Transfer, Academic Press, 1978.

[33] P. Hartley, H. Thissen, T. Vaithianathan, H. Griesser, A surface masking technique for the determination of plasma polymer film thickness by AFM, Plasmas Polymers 5 (1) (2000) 47–60.

[34] G. Rosengarten, J. Cooper-White, G. Metcalfe, Design and experimental issues with heat exchangers for microfluidics, in: 15th Australasian Fluid Mechanics Conference, University of Sydney, Sydney, 2004, AFMC00219 35.

[35] J.P. Chiou, The advancement of compact heat exchanger theory considering the effects of longitudinal heat conduction and flow nonuniformity, in Symposium on Compact Heat Exchangers, NY, ASME, 1980, pp. 101–121.

[36] D. Pachoud, A. Mitchell, G. Rosengarten. Microfluidic device with integrated temperature control unit for actuation of hydrogel, in: SPIE International Symposium on Smart Materials and Nano, Micro Smart Systems, Sydney, SPIE, 2004, pp. 5651–5664.

[37] G.L. Morrison, G. Rosengarten, M. Behnia, Mantle heat exchangers for horizontal tank thermosyphon solar water heaters, Solar Energy 67 (1) (1999) 53–64.